Electronic Supplementary Information

Heterointerface enhanced NiFe LDH/V-Co_4N electrocatalysts for oxygen evolution reaction

Shuya Zhang,[†a] Lan Wang,[†a] Tianzhu Xie, [a] Qiming Chen, [a] Wenchao Peng, [a] Yang Li, [a] Fengbao Zhang [a] and Xiaobin Fan*[abc]

[a] *School of Chemical Engineering and Technology, State Key Laboratory of Chemical Engineering, Tianjin University, Tianjin, 300354, China.*

[b] *Haihe Laboratory of Sustainable Chemical Transformations, Tianjin 300192, China.*

[c] *Institute of Shaoxing, Tianjin University, Zhejiang 312300, China.*

† These authors contributed equally.

[*] *Corresponding authors.*

E-mail addresses: xiaobinfan@tju.edu.cn

Experimental Section

Materials

Cobaltous nitrate hexahydrate [$Co(NO_3)_2 \cdot 6H_2O$, 99.99%, Aladdin], ammonium metavanadate [NH_4VO_3, 99.99%, Aladdin], ammonium fluoride (NH_4F, AR, Aladdin) and urea [$CO(NH_2)_2$, AR, Macklin]. Nickel nitrate hexahydrate [$Ni(NO_3)_2 \cdot 6H_2O$, AR, Aladdin] and ferrous sulfate ($FeSO_4 \cdot 7H_2O$, AR, Heowns). Nickel foam (NF). Ethanol is provided by Aladdin Chemical Co., China. All the chemicals were used without further purification.

Synthesis of NiFe LDH/Co_4N@NF arrays

Co_4N@NF sample was obtained via a similar process to V-Co_4N@NF, except without the addition of the V source. NiFe LDH/Co_4N@NF was obtained via a similar process to NiFe LDH/V-Co_4N@NF, except replacing the substrate with Co_4N@NF as the working electrode.

Synthesis of NiFe LDH @NF arrays

NiFe LDH@NF was obtained by replacing the substrate with bare NF based on the above experimental parameters.

Synthesis of NiFe LDH+V-Co4N@NF arrays

The suspension containing 2.8 mg NiFe LDH was dropped onto the V-Co4N@NF substrate and dried naturally.

Materials characterization

The morphologies and elemental mappings of materials were characterized by scanning electron microscopy (SEM, S-4800, HITACHI) and transmission electron microscopy equipped with an energy-dispersive X-ray analyzer (JEOL JEM-2100, Japan). X-ray diffraction (XRD, D8-Focus, Bruker Axs) was utilized to characterize the phases composition of samples. X-ray photoelectron spectroscopy (XPS, ESCALAB 250 XI) was employed to reveal the electronic structure of the samples.

Electrochemical measurement

All electrochemical tests for OER performance were performed on the electrochemical workstation (CHI760) in 1 M KOH solution. During the measurements, the three-electrode test system was adopted, where the prepared materials were used directly as working electrodes, and carbon rod and Ag/AgCl electrode were used as counter electrode and reference electrode, respectively. All potentials were converted into potentials related to RHE using the following equation, $E(RHE) = E_{Ag/AgCl} + 0.197 + 0.059\ pH$. Firstly, 50 cycles of cyclic voltammetry (CV) were carried out at the scan rate of 50 mV s^{-1} to make the catalyst stabilized. Then, anodic polarization curves were obtained by utilizing cyclic voltammetry (CV) at a scan rate of 1 mV s^{-1} and 90% *iR* compensation. Note that the reverse sweep data of the anodic polarization were selected for analysis to avoid the interference of the oxidation peaks.[1] Cyclic voltammetry (CV) curves were collected at different sweep rates in the potential range of 0.16-0.33V vs. RHE, which were used to calculate the double-layer capacitance and further estimate the electrochemically surface area (ECSA). The Nyquist plots were collected at the potential of 0.45 V vs RHE in the frequency range of 1000000 HZ-0.01 HZ. The durability was evaluated with chronoamperometry measurements to assess the electrochemical stability of the catalyst.

Computational details

In this work, DFT calculations were performed by Vienna Ab initio Simulation Package (VASP) with the projector augmented wave (PAW) method. The exchange-related function utilized was Perdew-Burke-Ernzerhof (PBE). The cut-off energy specified by ENCUT was set to 500 eV for cell optimization and calculation of the electronic structure. The modeling was performed with a vacuum spacing of at least 15 Å in the direction of the vertical catalyst surface to prevent interference. Taking into account the large structural model, the Brillouin zone integration was performed using 1 × 1 × 1 Monkhorst-Pack k-point sampling for primitive cells. To improve the calculation accuracy, the value of parameter EDIFF was set to 10^{-5} eV. The relaxation was stopped when the norms of all the forces are smaller than 0.02 eV/Å.

According to the OER mechanism proposed by Nørskov,[2] the reaction is a four-electron transfer process and each elemental step of the process is listed in equations (1) to (4), which involve the adsorption and desorption of reaction intermediates (such as *OH, *O, and *OOH) on the active sites of catalyst surface (denoted with *).

$$*+OH^- \rightarrow *OH+e^- \quad (1)$$

$$*OH+OH^- \rightarrow *O+H_2O+e^- \quad (2)$$

$$*O+OH^- \rightarrow *OOH+e^- \quad (3)$$

$$*OOH+OH^- \rightarrow O_2+H_2O+e^- \quad (4)$$

The Gibbs free energy of the four elemental steps can be calculated according to the following reduced equation (5) to (8). Where μ represents the chemical potential of the specified species, which can be calculated by DFT. U_{RHE} is the potential of the electrode relative to the RHE, where the value of U_{RHE} is chosen as 0 or 1.23 V.

$$\Delta G_1=\mu_{*_{OH}}-\mu_*-\mu_{H_2O(l)}+\frac{1}{2}\mu_{H_2(g)}-eU_{RHE} \quad (5)$$

$$\Delta G_2=\mu_{*_O}-\mu_{*_{OH}}-\mu_{H_2O(l)}+\frac{1}{2}\mu_{H_2(g)}-eU_{RHE} \quad (6)$$

$$\Delta G_3=\mu_{*_{OOH}}-\mu_{*_O}-\mu_{H_2O(l)}+\frac{1}{2}\mu_{H_2(g)}-eU_{RHE} \quad (7)$$

$$\Delta G_4=\mu_*-\mu_{*_{OOH}}+\mu_{O_2(g)}+\frac{1}{2}\mu_{H_2(g)}-eU_{RHE} \quad (8)$$

The theoretical overpotential can be calculated by the following equation.

$$\eta=\frac{\max[\Delta G_1,\Delta G_2,\Delta G_3,\Delta G_4]}{e}-1.23V \quad (9)$$

TOF calculation

TOF is calculated according to the following formula:

$$TOF=\frac{\text{number of total oxygen turnovers/ cm}^2}{\text{number of active sites /cm}^2}$$

Firstly, the electrochemical surface area (A_{ECSA}) was calculated according to the following equation:

$A_{ECSA}=\frac{\text{specific capacitance}}{40\ \mu F\ cm^{-2}\ per\ cm^2_{ECSA}}$, where specific capacitance is C_{dl} calculated from CV cures, and 40 μF is a constant to convert capacitance to A_{ECSA}.

Then, number of O_2 = $(j\frac{mA}{cm^{-2}})$ $(\frac{1\ C\ s^{-1}}{1000mA})$ $(\frac{1\ mol\ e^-}{96485.3\ C})$ $(\frac{1\ mol\ O_2}{4\ mol\ e^-})$ $(\frac{6.022\times10^{23}O_2\ molecules}{1\ mol\ O_2})$

= $1.56\times10^{15}\frac{O_2/s}{cm^{-2}}$ per $\frac{mA}{cm^{-2}}$

Number of active sites = $\left(\frac{\text{number of atoms/ unit cell}}{\text{volume/unit cell}}\right)^{\frac{2}{3}}$

Finally, the TOF plot was drawn according to the following equation:

TOF = $\frac{(1.56\times10^{15}\frac{O_2/s}{cm^{-2}}\text{ per }\frac{mA}{cm^{-2}})\times|j|}{\text{number of active sits}\times A_{ECSA}}$

Mass activity calculation

The Mass activity was calculated according to the following formulas:

$$\text{Mass activty} = \frac{j \times A}{m}$$

Where j (A cm^{-2}) was the measured current density at η=270 mV, A (cm^2) was the geometric area of the work electrode and m (g) referred to the total metal loading obtained by ICP-OES.

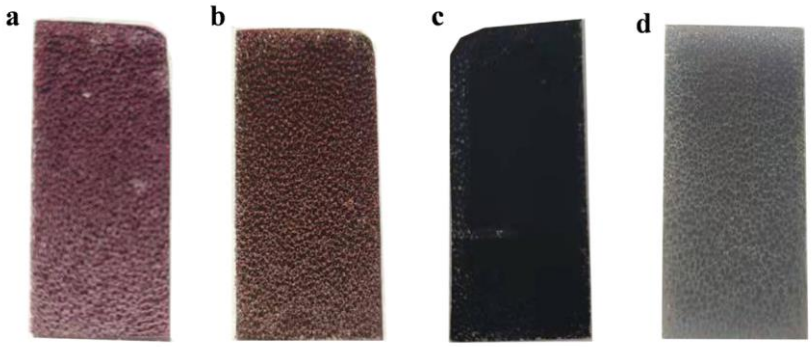

Fig. S1. The photos of different samples. (a) $Co(OH)_2$@NF. (b) V-$Co(OH)_2$@NF. (c) V-Co_4N@NF. (d) NiFe LDH/V-Co_4N@NF.

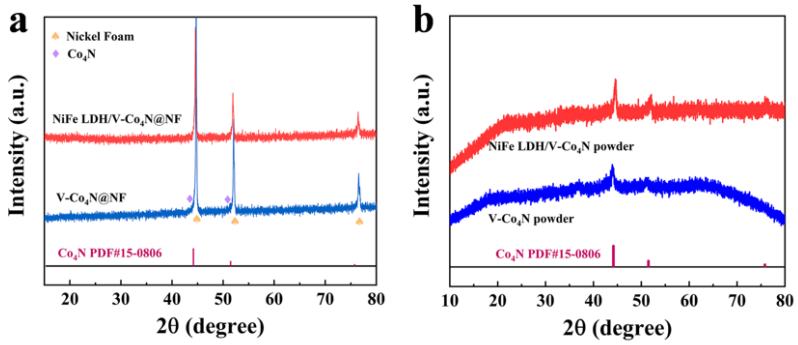

Fig. S2. XRD pattern of samples. (a) V-Co_4N@NF and NiFe LDH/V-Co_4N@NF. (b) V-Co_4N and NiFe LDH/V-Co_4N powder.

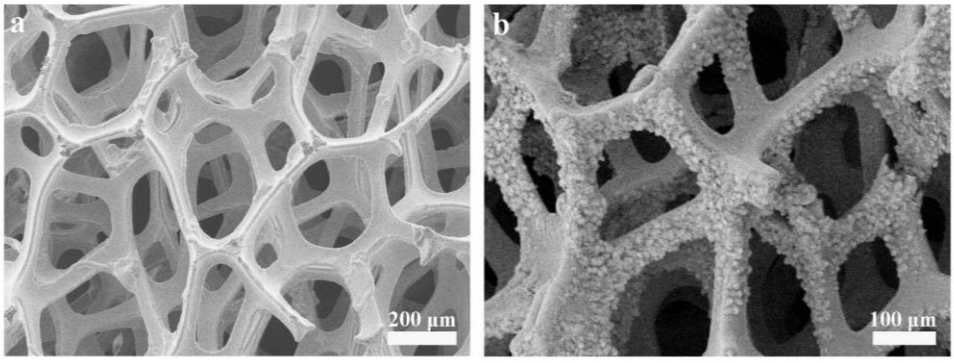

Fig. S3. SEM images. (a) Nickel foam substrate (NF). (b) V-$Co(OH)_2$@NF.

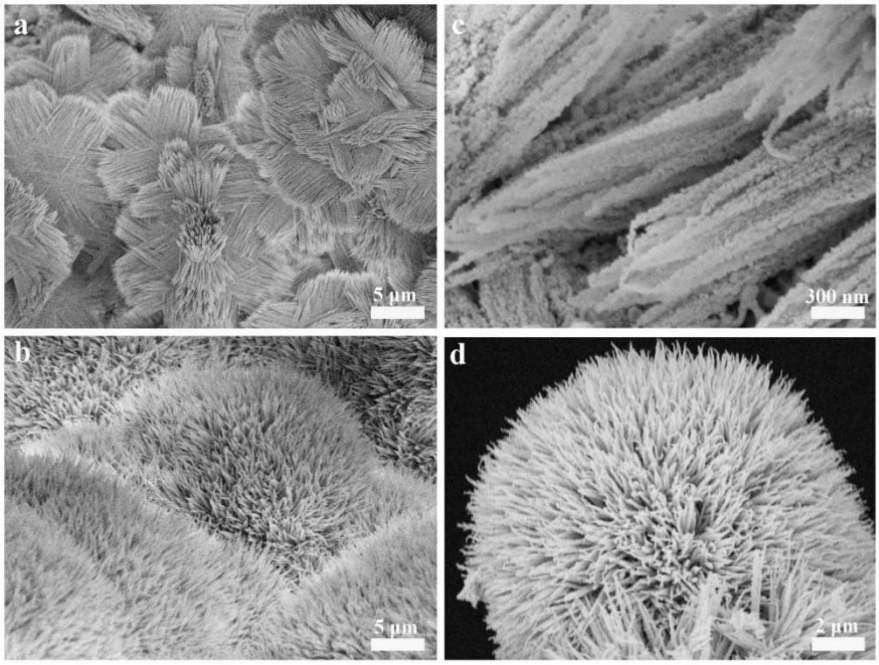

Fig. S4. SEM images. (a) $Co(OH)_2$@NF. (b) V-$Co(OH)_2$@NF. (c) Co_4N@NF. (d) V-Co_4N@NF.

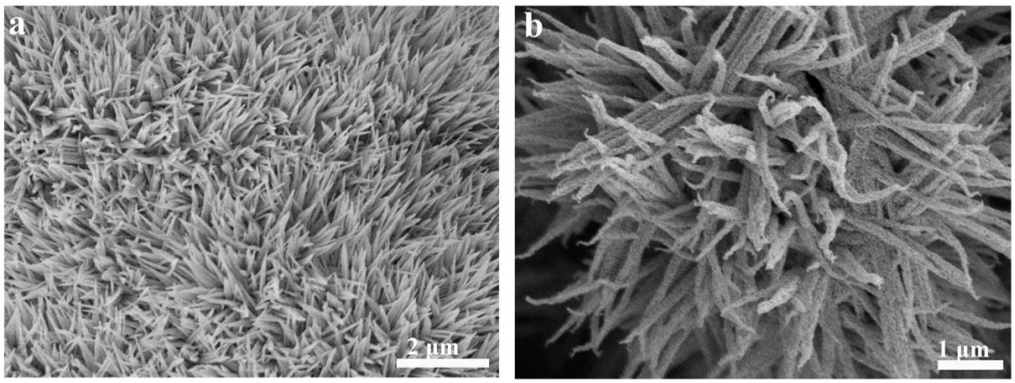

Fig. S5. SEM images. (a) V-$Co(OH)_2$@NF. (b) V-Co_4N@NF.

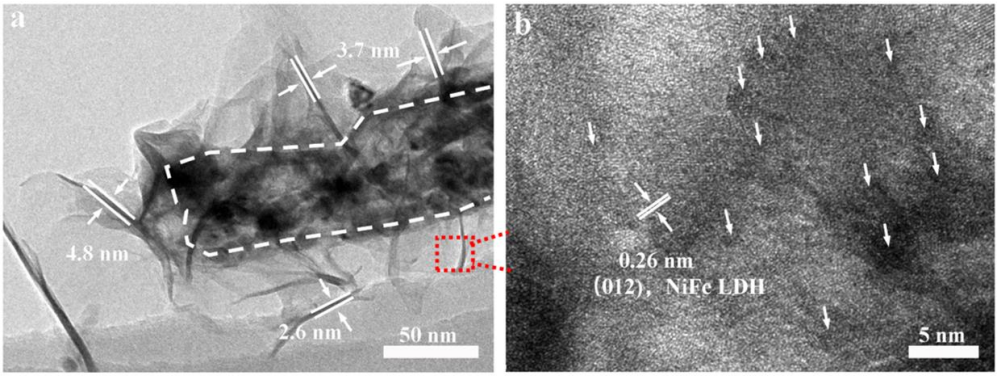

Fig. S6. TEM images. (a) NiFe LDH/V-Co_4N. (b) HRTEM image of NiFe LDH/V-Co_4N taken from the red square in the image on the left.

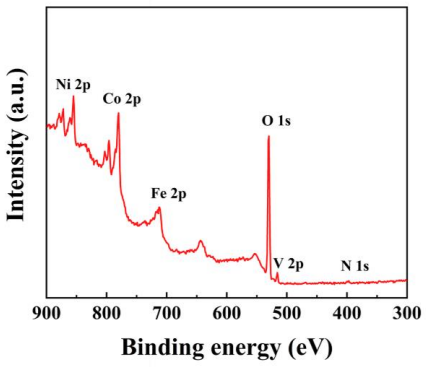

Fig. S7. XPS survey spectra of NiFe LDH/V-Co_4N.

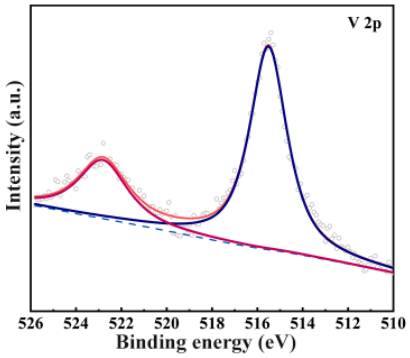

Fig. S8. (a) V 2p XPS spectra of V-Co_4N.

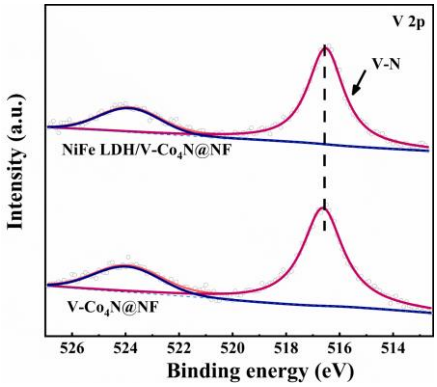

Fig. S9. V 2p XPS spectra before and after heterointerface formation.

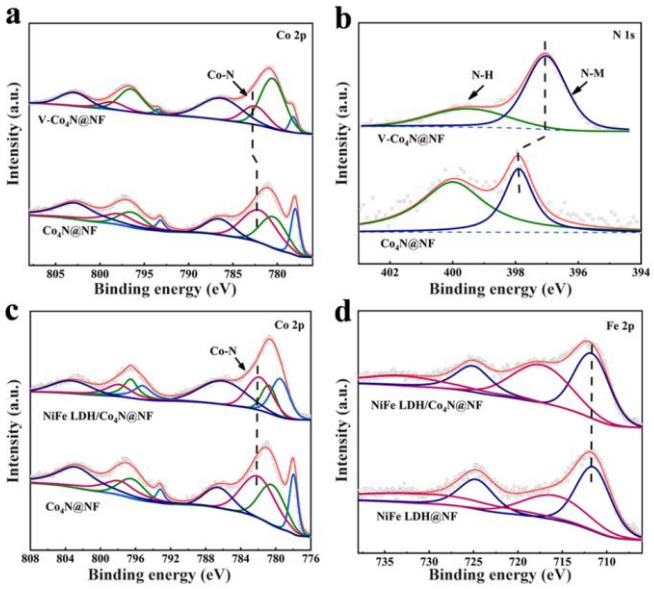

Fig. S10. Structural characterization. (a) Co 2p of Co_4N and V-Co_4N. (b) N 1s of Co_4N and V-Co_4N. (c) Co 2p of Co_4N and NiFe LDH/Co_4N. (d) Fe 2p of NiFe LDH and NiFe LDH/Co_4N.

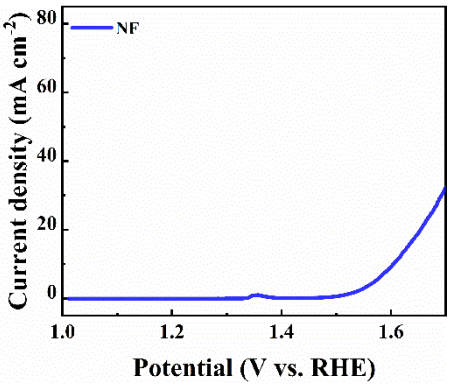

Fig. S11. LSV curve of pure nickel foam.

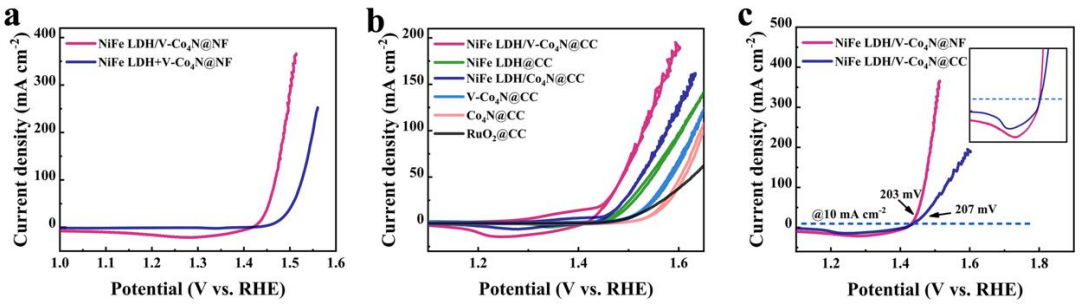

Fig. S12. (a) The anodic polarization curves of NiFe LDH/V-Co4N@NF and NiFe LDH+V-Co4N@NF. (b) The anodic polarization curves of catalysts loaded carbon cloth. (c) The comparison of overpotential at 10 mA cm^{-2} between NiFe LDH/V-Co4N@NF and NiFe LDH/V-Co4N@CC.

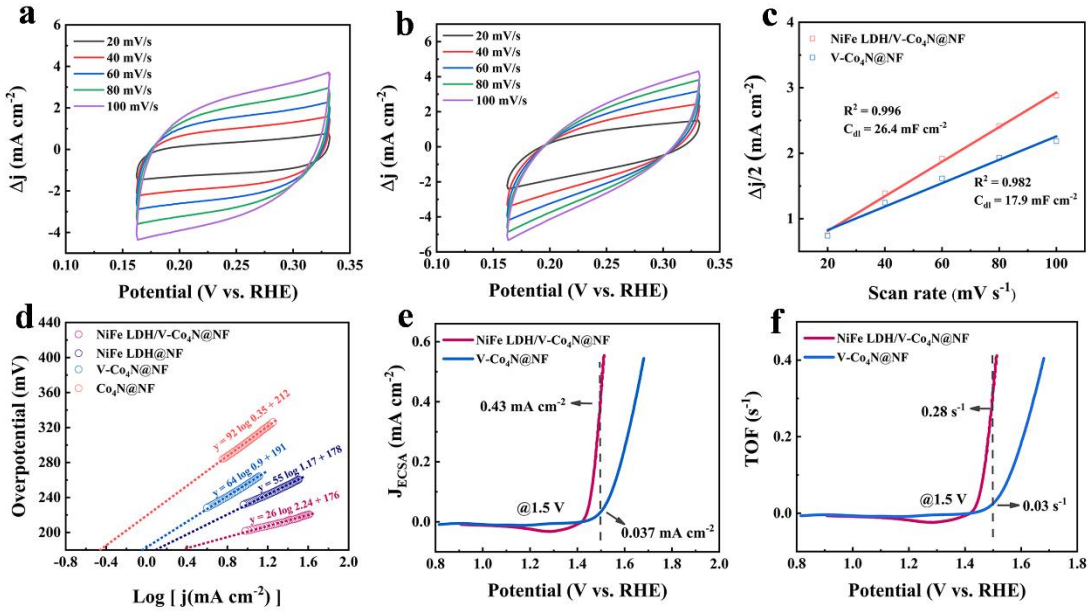

Fig. S13. (a) and (b) CV curves of NiFe LDH/V-Co_4N and V-Co_4N at different scan rates. (c) Calculated double-layer capacitance of different catalysts from CV curves. (d) Exchange current densities values derived from the Tafel plot. (e) ECSA normalized polarization curves of the NiFe LDH/V-Co_4N and V-Co_4N catalysts. (f) Turnover frequency (TOF) curves of the NiFe LDH/V-Co_4N and V-Co_4N catalysts. The number of total O_2 turnovers and active sites was calculated according to the references.[3-5]

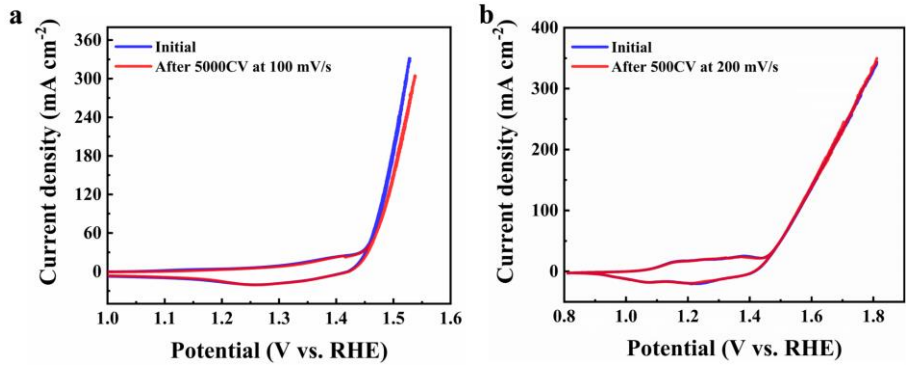

Fig. S14. Polarization curves of NiFe LDH/V-Co_4N@NF before and after dynamic stability test. (a) 5000 cycles CV test at the scan rate of 100 mV s^{-1}. (b) 500 cycles CV test at a scan rate of 200 mV s^{-1}.

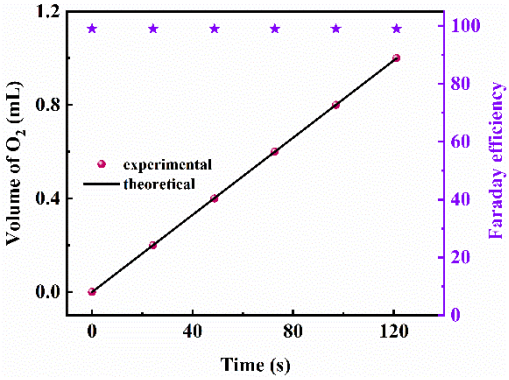

Fig. S15. The evaluation of Faradic efficiency for NiFe LDH/V-Co_4N@NF.

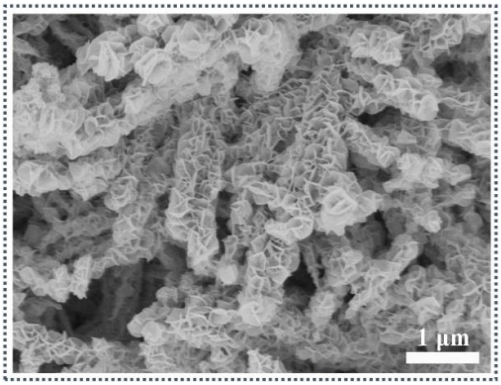

Fig. S16. SEM image of NiFe LDH/V-Co_4N@NF catalyst after OER test.

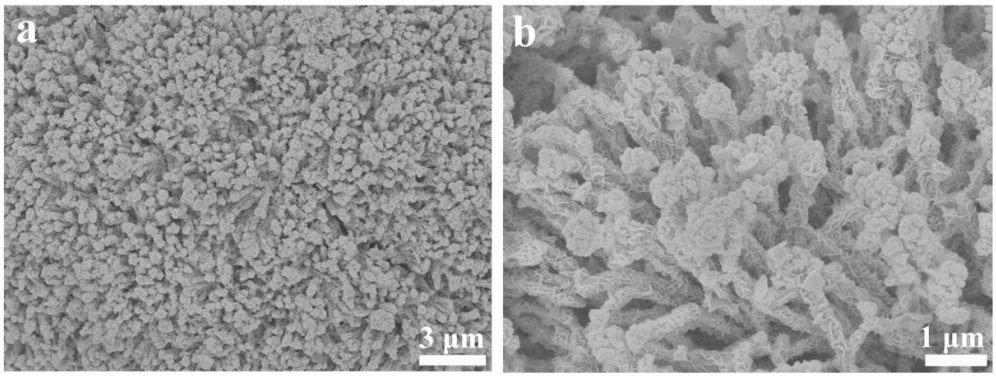

Fig. S17. SEM images of NiFe LDH/V-Co_4N@NF after 24 h stability test.

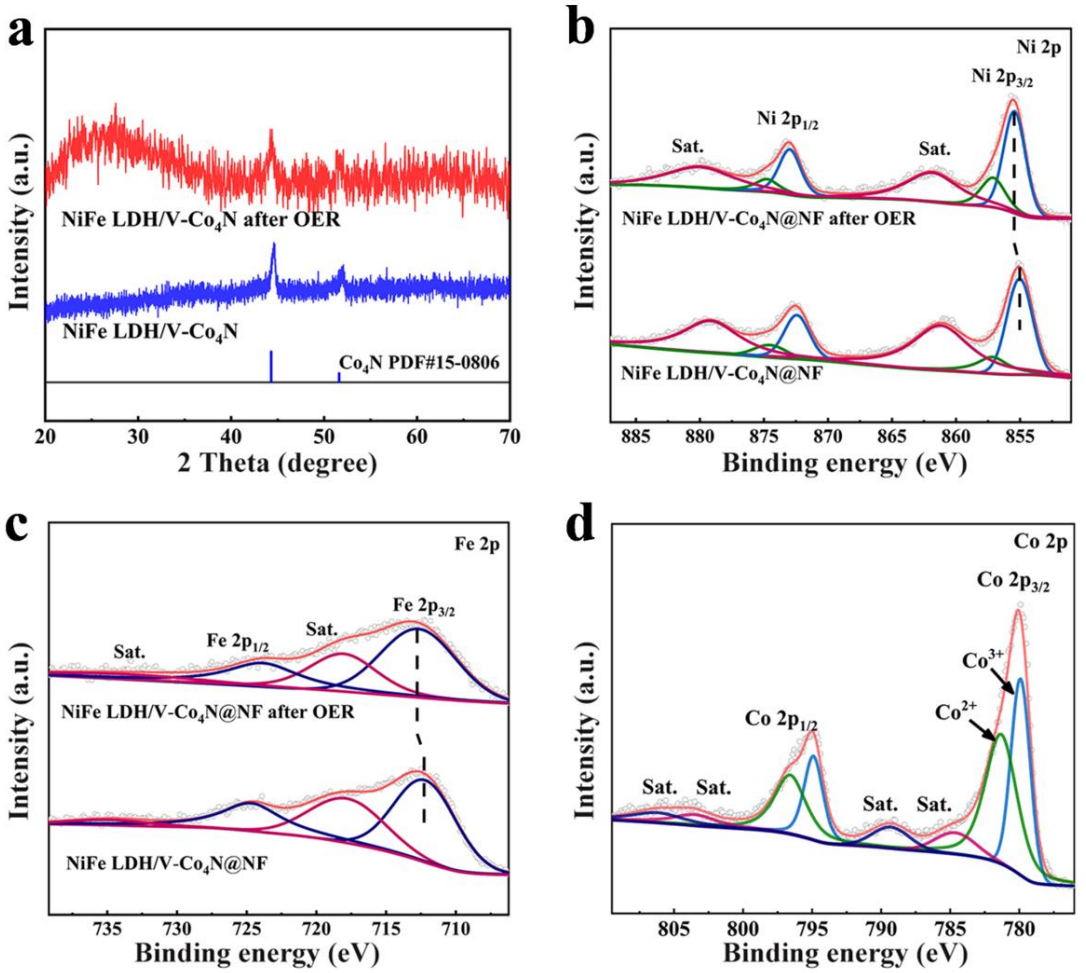

Fig. S18. Characterization of the catalyst after 24 h stability test. (a) XRD pattern without NF. (b) Ni 2p XPS of NiFe LDH/V-Co_4N before and after stability test. (c) Fe 2p XPS of NiFe LDH/V-Co_4N before and after stability test. (d) Co 2p XPS after stability test.

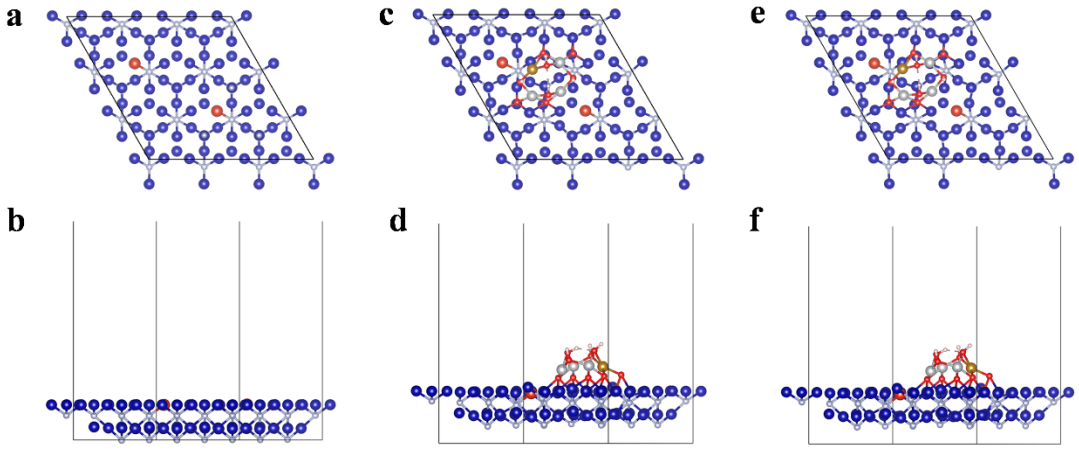

Fig. S19. Structural models. (a) and (b) optimized V-Co_4N. (c) and (d) NiFe LDH/V-Co_4N before optimization. (e) and (f) NiFe LDH/V-Co_4N after optimization. The blue ball represents the Co atom, the brown ball represents the Fe atom, the small red ball represents the O atom, the small pink ball represents the H atom, the big gray ball represents Ni atoms, the small gray ball represents N atoms and the large red ball represents the V atom.

		V-Co_4N	NiFe LDH/Co_4N	NiFe LDH/V-Co_4N
OH*	Top view	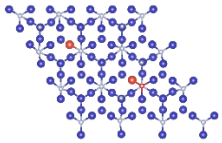	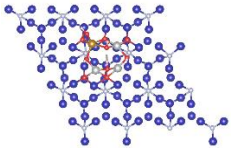	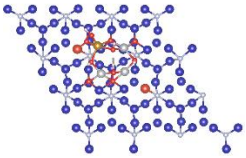
	Front view	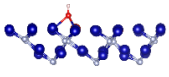	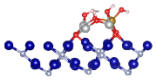	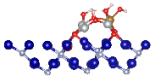
O*	Top view	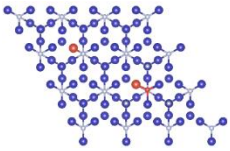	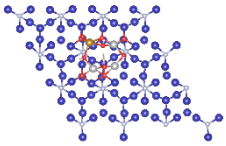	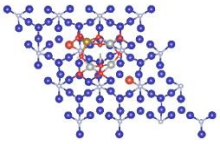
	Front view	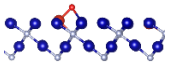	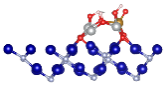	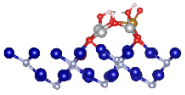
OOH*	Top view	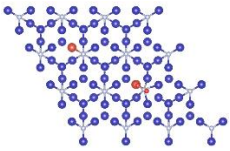	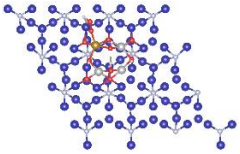	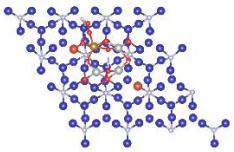
	Front view	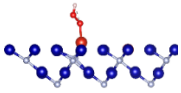	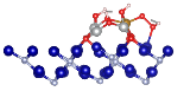	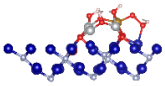

Fig. S20. Geometric adsorption configurations of oxygenated intermediates （*OH, *O, and *OOH）on active site V-Co_4N (Co site), NiFe LDH/Co_4N (Fe site), and NiFe LDH/V-Co_4N (Fe site) electrocatalyst surface from different views.

NiFe LDH/V-Co_4N (Ni site)	OH*	O*	OOH*
Top view	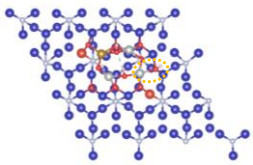	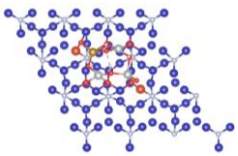	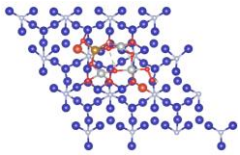
Front view	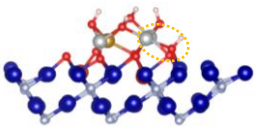	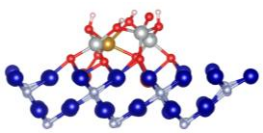	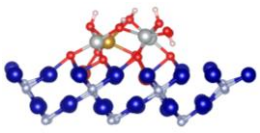

Fig. S21. Geometric adsorption configurations of oxygenated intermediates （*OH, *O, and *OOH）at Ni site of NiFe LDH/V-Co_4N.

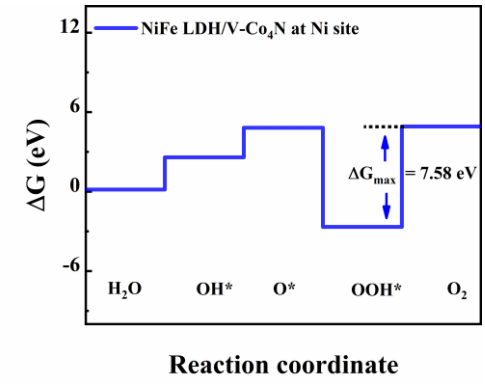

Fig. S22. Gibbs free energy diagram for the four steps of OER at Ni site of NiFe LDH/Co_4N.

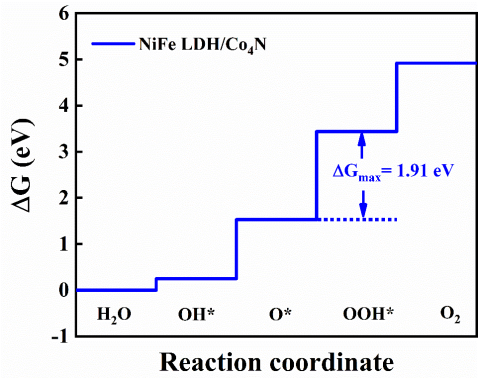

Fig. S23. Gibbs free energy diagram for the four steps of OER on NiFe LDH/Co_4N.

The rate-determining step for the NiFe LDH/Co_4N catalyst is also the third step, and the calculated overpotential is 0.68 V. The value of the overpotential is between that of Co_4N and NiFe LDH/V-Co_4N, which is consistent with the trend of the overpotential obtained from electrochemical experimental tests. This indicates that the interfacial interaction between NiFe LDH and Co_4N is non-competitive compared to that between NiFe LDH and V-Co_4N.

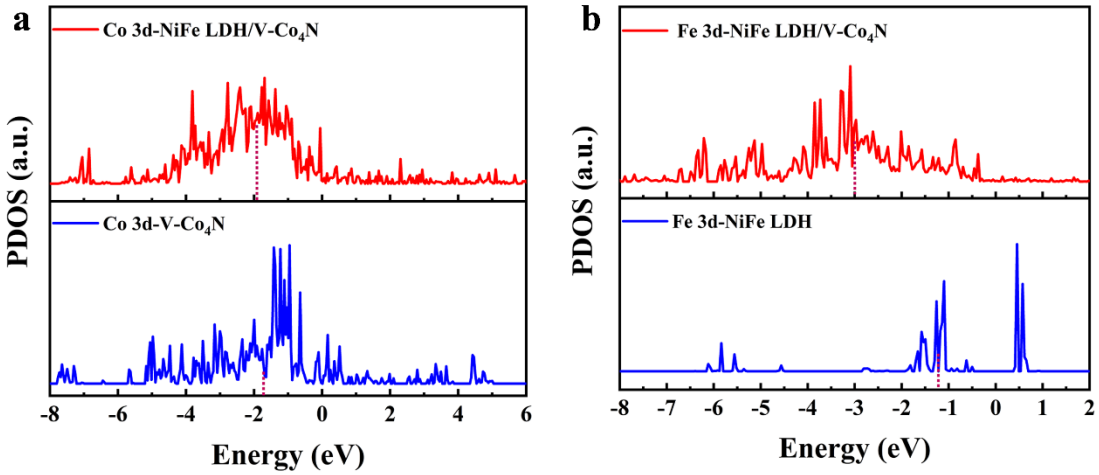

Fig. S24. Local density of states of surface-specific atoms. (a) Co d orbitals of NiFe LDH/V-Co_4N and V-Co_4N. (b) Fe d orbitals of NiFe LDH/V-Co_4N and NiFe LDH. The dotted line represents the position of the d-band center.

The change in the d-band center levels of the surface Co and Fe atoms indicates the existence of electronic coupling effects at the interface after compositing.

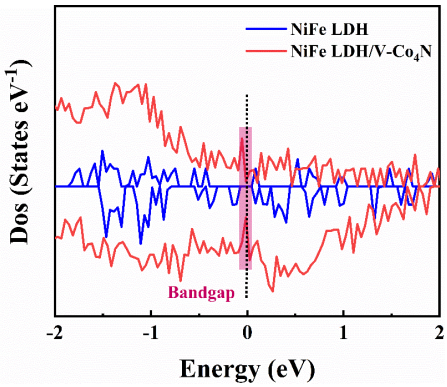

Fig. S25. Total density of states curves of NiFe LDH/V-Co_4N and NiFe LDH. Fermi-level is set to zero.

Table S1 The metal loading of fresh NiFe LDH/V-Co_4N on NF.

elements	V	Fe	Co	Ni
loading amount W (%)	2.56%	1.15%	30.80%	40.87%
loading amount (mg/cm^2)	0.13	0.06	1.54	2.04

Table S2 Comparison of OER performance for the samples of this work and reported catalysts (η_{10}-overpotential at 10 mA cm^{-2} with *iR* correction, η_{100}-overpotential at 100 mA cm^{-2} with *iR* correction).

Catalysts	Electrolyte	η_{10} (mV)	η_{100} (mV)	Tafel slope (mV dec^{-1})	Ref.
NiFe LDH/V-Co_4N@NF	1 M KOH	203	240	26.0	This work
Ni_3N-NiMoN/CC	1 M KOH	277	/	67	6
FeCo-Co_4N/N-C	1 M KOH	280	/	40	7
Ni_2Mo_3N	0.1 M KOH	270	/	59	8
$Co_4N_{0.82}$ nanosheets	1 M KOH	190	/	84	9
CoO_x@CoN_y/NCNF	1 M KOH	460	/	85.6	10
CoVFeN@ NF	1 M KOH	212	/	34.8	11
NiMoN@NiFeN	1 M KOH	/	277	58.6	12
CoFe-NA/NF	1 M KOH	/	250	69.9	13
Co_4N-CeO_2/GP	1 M KOH	239	/	37.1	14
CoNiN@NiFe LDH	1 M KOH	227	/	73.6	15
CoSAs-MoS_2/TiN	1 M KOH	340	/	81.2	16
(N, S)-RGO@CoN	1 M Na_2SO4	220	/	33	17
TiN@$Co_{5.47}N$	1 M KOH	211	/	42.5	18
WN-$Ni(OH)_2$	1 M KOH	/	339	96.5	19
FeOOH/Ni_3N	1 M KOH	244	/	64	20
Co_4N NW/CC	1 M KOH	257	/	44	21

Table S3 Comparison of OER performance between this work and NiFe LDH-based catalysts (η_{10}-overpotential at 10 mA cm^{-2}).

Catalysts	Electrolyte	η_{10} (mV)	Tafel slope (mV dec^{-1})	Ref.
NiFe LDH/V-Co_4N@NF	1 M KOH	203	26.0	This work
PM-NiFe LDH	1 M KOH	230	47	[22]
NiFe LDH-NS@DG10	1 M KOH	210	52	[23]
Ru-NiFe LDH	1 M KOH	246	67.2	[24]
IrO_x/U-NiFe LDH	1 M KOH	236	74.3	[25]
CeO_{2-x}/NiFe LDH	1 M KOH	216	74.1	[26]
Co@NiFe LDH	1 M KOH	253	44	[27]
NiFe LDH	1 M KOH	247	37	[28]
NiFeCo LDH/CF	1 M KOH	249	42	[29]
(EE)NiFe-LDH nanosheets	1 M KOH	205	50.8	[30]
CoO@NiFe LDH/NF	1 M KOH	210	83	[31]
Co-C@NiFe LDH	1 M KOH	249	57.9	[32]
Ultrathin NiFe LDH	1 M KOH	210	31	[33]
F-NiFe LDH	1 M KOH	243	50	[34]
LDH-Bir	1 M KOH	258	43	[35]

Table S4 The comparison of NiFe LDH/V-Co_4N@NF with commercial catalyst RuO_2 at overpotential of 270 mV.

catalysts	Mass activity (A g^{-1})	Surface activity (mA cm^{-2})	Turnover frequency (s^{-1})
NiFe LDH/V-Co_4N@NF (This work)	78	282.6	0.7
RuO_2	6.8	5.4	0.4

Table S5 The composition of the element and catalyst loading amount after stability test.

elements	V	Fe	Co	Ni
loading amount W (%)	1.66%	3.65%	35.34%	24.63%

Table S6 Gibbs free energy of the intermediate reactions at each step of the OER process and theoretically calculated overpotentials for V-Co_4N, NiFe LDH/Co_4N, and NiFe LDH/V-Co_4N.

Samples	**$\triangle G_{I}$**	**$\triangle G_{II}$**	**$\triangle G_{III}$**	**$\triangle G_{IV}$**	**Overpotential (V)**
V-Co_4N	0.24	0.35	2.93	1.40	1.70
NiFe LDH/Co_4N	0.25	1.28	1.91	1.48	0.68
NiFe LDH/V-Co_4N	0.19	1.48	1.82	1.43	0.59

Table S7 The d-band center (ε_d) levels of the surface atoms in the different structures, where VCN represents V-Co_4N, LVCN represents NiFe LDH/V-Co_4N.

Structures	Co 3d-VCN	Fe 3d-LDH	Co 3d-LVCN	Fe 3d-LVCN
d-band center (ε_d)/eV	–1.749	–1.224	–1.939	–3.024

References

1 X. Xu, F. Song and X. Hu, *Nat. Commun.*, 2016, **7**, 12324.

2 I. C. Man, H. Y. Su, F. Calle‐Vallejo, H. A. Hansen, J. I. Martínez, N. G. Inoglu, J. Kitchin, T. F. Jaramillo, J. K. Nørskov and J. Rossmeisl, *ChemCatChem*, 2011, **3**, 1159-1165.

3 Z. Chen, Y. Song, J. Cai, X. Zheng, D. Han, Y. Wu, Y. Zang, S. Niu, Y. Liu, J. Zhu, X. Liu and G. Wang, *Angew. Chem. Int. Ed.*, 2018, **57**, 5076-5080.

4 X. Yu, J. Zhao and M. Johnsson, *Adv. Funct. Mater.*, 2021, **31**, 2101578.

5 X.-D. Wang, Y.-F. Xu, H.-S. Rao, W.-J. Xu, H.-Y. Chen, W.-X. Zhang, D.-B. Kuang and C.-Y. Su, *Energy Environ. Sci.*, 2016, **9**, 1468-1475.

6 A. Wu, Y. Xie, H. Ma, C. Tian, Y. Gu, H. Yan, X. Zhang, G. Yang and H. Fu, *Nano Energy*, 2018, **44**, 353-363.

7 X. Zhu, T. Jin, C. Tian, C. Lu, X. Liu, M. Zeng, X. Zhuang, S. Yang, L. He, H. Liu and S. Dai, *Adv. Mater.*, 2017, **29**, 1704091.

8 Y. Yuan, S. Adimi, X. Guo, T. Thomas, Y. Zhu, H. Guo, G. S. Priyanga, P. Yoo, J. Wang, J. Chen, P. Liao, J. P. Attfield and M. Yang, *Angew. Chem. Int. Ed.*, 2020, **59**, 18036-18041.

9 H. Liu, J. Lei, S. Yang, F. Qin, L. Cui, Y. Kong, X. Zheng, T. Duan, W. Zhu and R. He, *Appl. Catal. B: Environ.*, 2021, **286**, 119894.

10 K. R. Yoon, C. K. Hwang, S. H. Kim, J. W. Jung, J. E. Chae, J. Kim, K. A. Lee, A. Lim, S. H. Cho, J. P. Singh, J. M. Kim, K. Shin, B. M. Moon, H. S. Park, H. J. Kim, K. H. Chae, H. C. Ham, I. D. Kim and J. Y. Kim, *ACS Nano*, 2021, **15**, 11218–11230.

11 D. Liu, H. Ai, J. Li, M. Fang, M. Chen, D. Liu, X. Du, P. Zhou, F. Li, K. H. Lo, Y. Tang, S. Chen, L. Wang, G. Xing and H. Pan, *Adv. Energy Mater.*, 2020, **10**, 2002464.

12 L. Yu, Q. Zhu, S. Song, B. McElhenny, D. Wang, C. Wu, Z. Qin, J. Bao, Y. Yu, S. Chen and Z. Ren, *Nat. Commun.*, 2019, **10**, 5106.

13 M. Chen, D. Liu, B. Zi, Y. Chen, D. Liu, X. Du, F. Li, P. Zhou, Y. Ke, J. Li, K. H. Lo, C. T. Kwok, W. F. Ip, S. Chen, S. Wang, Q. Liu and H. Pan, *J. Energy Chem.*, 2022, **65**, 405-414.

14 H. Sun, C. Tian, G. Fan, J. Qi, Z. Liu, Z. Yan, F. Cheng, J. Chen, C. P. Li and M. Du, *Adv. Funct. Mater.*, 2020, **30**, 1910596.

15 J. Wang, G. Lv and C. Wang, *Appl. Surf. Sci.*, 2021, **570**, 151182.

16 T. L. L. Doan, D. C. Nguyen, S. Prabhakaran, D. H. Kim, D. T. Tran, N. H. Kim and J. H. Lee, *Adv. Funct. Mater.*, 2021, **31**, 2100233.

17 D. Guo, Z. Zeng, Z. Wan, Y. Li, B. Xi and C. Wang, *Adv. Funct. Mater.*, 2021, **31**, 2101324.

18 D. Guo, Z. Wan, Y. Li, B. Xi and C. Wang, *Adv. Funct. Mater.*, 2020, **31**, 2008511.

19 C. Lv, X. Wang, L. Gao, A. Wang, S. Wang, R. Wang, X. Ning, Y. Li, D. W. Boukhvalov, Z. Huang and C. Zhang, *ACS Catal.*, 2020, **10**, 13323-13333.

20 J. Guan, C. Li, J. Zhao, Y. Yang, W. Zhou, Y. Wang and G.-R. Li, *Appl. Catal. B: Environ.*, 2020, **269**, 118600.

21 P. Chen, K. Xu, Z. Fang, Y. Tong, J. Wu, X. Lu, X. Peng, H. Ding, C. Wu and Y. Xie, *Angew. Chem. Int. Ed.*, 2015, **54**, 14710-14714.

22 X. Zhang, Y. Zhao, Y. Zhao, R. Shi, G. I. N. Waterhouse and T. Zhang, *Adv. Energy Mater.*, 2019, **9**, 1900881.

23 Y. Jia, L. Zhang, G. Gao, H. Chen, B. Wang, J. Zhou, M. T. Soo, M. Hong, X. Yan, G. Qian, J. Zou, A. Du and X. Yao, *Adv. Mater.*, 2017, **29**, 1700017.

24 Y. Yang, W.-J. Wang, Y.-B. Yang, P.-F. Guo, B. Zhu, K. Wang, W.-T. Wang, Z.-H. He and Z.-T. Liu, *J. Electrochem. Soc.*, 2022, **169**, 024503.

25 D. Liu, Y. Du, T. Li, H. Zhang, D. Liu, W. Zhang, H. Tang, Y. Hou, J. Li, S. Yan, T. Yu and Z. Zou, *Chem. Commun.*, 2020, **56**, 11465-11468.

26 Y. Du, D. Liu, T. Li, Y. Yan, Y. Liang, S. Yan and Z. Zou, *Appl. Catal. B: Environ.*, 2022, **306**, 121146.

27 S. Liu, R. Wan, Z. Lin, Z. Liu, Y. Liu, Y. Tian, D.-D. Qin and Z. Tang, *J. Mater. Chem. A*, 2022, **10**, 5244-5254.

28 H. Koshikawa, H. Murase, T. Hayashi, K. Nakajima, H. Mashiko, S. Shiraishi and Y. Tsuji, *ACS Catal.*, 2020, **10**, 1886-1893.

29 Y. Lin, H. Wang, C. K. Peng, L. Bu, C. L. Chiang, K. Tian, Y. Zhao, J. Zhao, Y. G. Lin, J. M. Lee and L. Gao, *Small*, 2020, **16**, 2002426.

30 B. Wang, X. Han, C. Guo, J. Jing, C. Yang, Y. Li, A. Han, D. Wang and J. Liu, *Appl. Catal. B: Environ.*, 2021, **298**, 120580.

31 Z. Wang, J. Zhang, Q. Yu, H. Yang, X. Chen, X. Yuan, K. Huang and X. Xiong, *Chem. Eng. J.*, 2021, **410**, 128366.

32 W. Li, S. Chen, M. Zhong, C. Wang and X. Lu, *Chem. Eng. J.*, 2021, **415**, 128879.

33 C. Kuai, Y. Zhang, D. Wu, D. Sokaras, L. Mu, S. Spence, D. Nordlund, F. Lin and X.-W. Du, *ACS Catal.*, 2019, **9**, 6027-6032.

34 C. Wu, H. Li, Z. Xia, X. Zhang, R. Deng, S. Wang and G. Sun, *ACS Catal.*, 2020, **10**, 11127-11135.

35 X. Long, Z. Chen, M. Ju, M. Sun, L. Jin, R. Cai, Z. Wang, L. Dong, L. Peng, B. Huang and S. Yang, *Angew. Chem. Int. Ed.*, 2021, **60**, 9699-9705.